RSC Advances

PAPER

View Article Online
View Journal | View Issue

Cite this: *RSC Adv.*, 2016, **6**, 44333

Hydrogenation of cinnamaldehyde to hydrocinnamaldehyde over Pd nanoparticles deposited on nitrogen-doped mesoporous carbon†

Atul S. Nagpure, Lakshmiprasad Gurrala, Pranjal Gogoi and Satyanarayana V. Chilukuri*

Received 15th February 2016
Accepted 28th April 2016

DOI: 10.1039/c6ra04154j

www.rsc.org/advances

Palladium nanoparticles deposited on nitrogen-doped mesoporous carbon (NMC) were synthesized by simple ultrasonic-assisted method. This novel Pd-NMC catalyst was highly active and selective for the hydrogenation of cinnamaldehyde (CA) to hydrocinnamaldehyde (HCA) at room temperature (30 °C) under low H_2 pressure. The nitrogen-free mesoporous carbon (MC) and activated carbon (AC) were also employed as the support for Pd in the liquid-phase hydrogenation of CA. The incorporation of nitrogen into carbon matrix remarkably enhanced the catalytic activity and C=C bond hydrogenation selectivity (HCA selectivity of 93% with 100% CA conversion for Pd-NMC) in CA hydrogenation compared to the catalysts with no nitrogen (HCA selectivity of 66 and 47% for Pd-MC and Pd-AC, respectively). Moreover, Pd-NMC catalyst demonstrated an excellent recyclability without any loss in activity and HCA selectivity when it was reused for six times. The superior catalytic performance of Pd-NMC catalyst in CA hydrogenation is attributed to the small size of Pd nanoparticles due to presence of high nitrogen content (11.6 wt%) and mesoporous nature of NMC support.

1. Introduction

Chemoselective hydrogenation of α,β-unsaturated carbonyl compounds into their corresponding unsaturated alcohols and saturated carbonyls over heterogeneous catalysts has drawn increasing attention for both scientific and economic reasons.[1] As a representative of α,β-unsaturated aldehyde, cinnamaldehyde (CA) is particularly vital as it can be selectively hydrogenated to hydrocinnamaldehyde (HCA) or cinnamyl alcohol (CAL), depending on whether C=C bond is hydrogenated or the C=O bond (Scheme 1). HCA and CAL are very important intermediates for the synthesis of many fine chemicals, perfumes and pharmaceuticals.[2] HCA was found to be essential intermediate in the preparation of a drug used in the treatment of HIV.[2]

Supported Pt,[3a–e] Au,[3f] Ru,[3g–h] Ir,[3i–j] Co[3k] and Cu[3l–m] catalysts were reportedly active for the selective hydrogenation of CA to CAL. Various supported metal catalysts were employed for the hydrogenation of CA to get HCA with high selectivity.[4] Mahmoud *et al.* achieved 100% CA conversion and 75% HCA selectivity over Pd/SiO_2 catalyst.[2b] Ledoux *et al.* studied selective hydrogenation of CA to HCA over Pd catalyst supported on carbon nanofibers.[4a] Conversion of CA was 100% at 98% HCA selectivity when the reaction was carried out at 80 °C for nearly 30 h. Liu *et al.* reported 91.3% HCA selectivity at 98.6% CA conversion over Pd supported on multiwalled carbon nanotubes under 40 bar H_2 and 148 bar CO_2 pressure at 60 °C.[4b] Arai *et al.* obtained 87% HCA selectivity and 100% CA conversion using Pd/C catalyst under 40 bar H_2 and 80 bar CO_2 pressure.[4c] Amadou *et al.* achieved 90% HCA selectivity at nearly 100% CA conversion over Pd supported on nitrogen-doped carbon nanotubes at 80 °C in 8 h.[4d] Begin *et al.* used few-layer graphene supported Pd catalyst to obtained 92% HCA selectivity and almost 100% CA conversion at 80 °C.[4e] Giambastiani *et al.* reported 97% HCA selectivity and 100% CA conversion by using $Pd/\gamma\text{-}Al_2O_3$ catalyst at 100 °C in 3 h.[4f] Zhang *et al.* studied CA hydrogenation over SiO_2 supported nickel phosphide catalyst and achieved 93% HCA selectivity and 78% CA conversion at

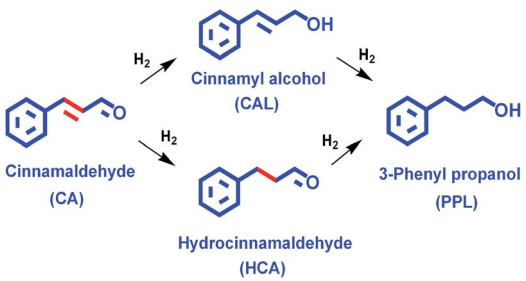

Scheme 1 Possible reaction pathways for hydrogenation of CA.

Catalysis & Inorganic Chemistry Division, CSIR-National Chemical Laboratory, Dr. Homi Bhabha Road, Pune-411008, India. E-mail: sv.chilukuri@ncl.res.in; Fax: +91-20-25902633; Tel: +91-20-25902019

† Electronic supplementary information (ESI) available. See DOI: 10.1039/c6ra04154j

120 °C.[4g] Marchi *et al.* reported 59.5% HCA selectivity with 60% CA conversion by using Cu/SiO_2 catalyst at 120 °C.[4h] However, obtaining high HCA selectivity at high conversion of CA, particularly at ambient reaction conditions and reusability of the catalyst are still important issues that need to be addressed.

The high activity and selectivity of catalysts in CA hydrogenation is a challenging task due to intricate reaction mechanisms involved including dissociative/non-dissociative, competitive adsorption as well as formation of coke, side reactions, adsorption of solvents, *etc.*[1c,2a,5] Although, many studies have been reported for the selective hydrogenation of CA to HCA, a more efficient catalyst system that is active even at room temperature and under low H_2 pressure is highly desirable.

Recent research efforts on carbon materials demonstrate their exceptional features (chemical and thermal stability, high surface area, *etc.*), as a new class of solid supports for a variety of heterogeneous catalysts.[6] However, noble metals (*e.g.*, Pd, Pt, Rh and Ru) deposited on carbon materials easily leach out during catalyst evaluation because of weak interaction between carbon surface and the metal nanoparticles. Moreover, the catalytic properties of porous carbons do not always satisfy all the requirements of a catalyst support. Hence, modification of carbons is essential in the majority of cases.[7] Usually, single-walled carbon nanotubes cannot efficiently anchor Pd nanoparticles without generation of defects.[8] In order to reinforce the interaction between metal and the support, carbons are generally oxidized with HNO_3 to introduce defects.[9] Nitrogen-doped carbon materials have attracted worldwide attention due to their outstanding performance in various applications, as catalyst supports,[10] for applications in supercapacitors,[11] for metal-free oxygen reduction reaction in case of fuel cell cathodes,[12] hydrogenation reaction,[13] *etc.* Doping with electron-rich nitrogen atoms in the carbon architecture can enhance electrical, chemical and functional properties.[14] Nitrogen-doped carbon materials show several features that are significantly different from their undoped counterparts. The presence of nitrogen atoms in the carbon matrix could also alter the electronic and chemical interactions with the deposited metal nanoparticles, which can really modify the overall catalytic activity as well as product selectivity.[4d]

Herein, we report a highly efficient and chemoselective Pd catalyst supported on nitrogen-doped mesoporous carbon (NMC) for the liquid-phase hydrogenation of CA to HCA. The Pd-NMC catalyst used in this investigation showed admirable catalytic activity (100% CA conversion) with high HCA selectivity (93%) under low H_2 pressure at room temperature (30 °C). Furthermore, Pd-NMC catalyst displayed an excellent reusability in the hydrogenation of CA to HCA.

2. Results and discussion

2.1. Structural characteristics of the catalysts

The NMC support was prepared by a colloidal silica nanocasting route (Scheme S1, ESI†), which involved the mixing of melamine–phenol–formaldehyde polymer sol with colloidal silica to obtain composite hydrogel.[15] Its subsequent carbonization in N_2 atmosphere at 800 °C and silica dissolution by treatment with NaOH gave the NMC with disordered mesopores. The elemental analysis showed that the resulting NMC has a high nitrogen content of 11.6 wt% (Table 1 and Table S1†). This as-synthesized NMC was used as a support for loading of Pd by a modified ultrasonic-assisted method (Scheme S2, ESI†).[13] A similar procedure was adopted for the preparation of activated carbon (AC) and mesoporous carbon (MC) supported Pd catalysts. The X-ray diffraction (XRD) pattern of NMC, Pd-NMC, Pd-AC and Pd-MC are shown in Fig. 1a. A broad diffraction peak at around $2\theta = 25.2°$ and a weak peak around 43.7° were observed for NMC, that correspond to the (002) and (100) crystal planes of graphite lattice, respectively.[15] The XRD pattern of Pd-NMC catalyst was similar to that of NMC and does not contain any diffraction peaks related to the metallic Pd, suggesting formation of highly dispersed Pd nanoparticles. The diffraction peaks of Pd in Pd-AC were weak. But, significantly sharp diffraction peaks of Pd at $2\theta = 40.1$, 46.7, 68.1 and 82.1° were detected in Pd-MC, which were assigned to (111), (200), (220) and (311) crystalline planes of metallic Pd, respectively. As shown in Fig. 1b, NMC, Pd-NMC and Pd-MC samples show type IV adsorption–desorption isotherms with a H2 hysteresis loop, corresponding to the typical mesoporous structure of the materials, while Pd-AC exhibits type II adsorption–desorption isotherm, related to the microporous nature of the sample. The other textural parameters and physico-chemical properties of the catalysts are summarized in Table 1.

Raman spectroscopy was employed to study the graphitic nature of the carbon (Fig. 1c). It consists of characteristic D- and G-bands of disordered graphitic carbon materials, at 1335 and

Table 1 Textural properties and Pd metal characteristics of the catalysts

Catalyst	Pd content[a] (wt%)	BET surface area ($m^2\ g^{-1}$)	Micropore surface area[b] ($m^2\ g^{-1}$)	Average pore diameter[c] (nm)	Nitrogen content[d] (wt%)	Average Pd particle size[e] (nm)	Pd metal dispersion[f] (%)	Pd metal surface area[g] ($m^2\ g^{-1}$)
NMC	—	844	103	12.4	11.6	—	—	—
Pd-NMC	2.05	791	85	12.2	11.5	2.4	54.0	4.15
Pd-MC	1.97	712	116	13.0	0	7.7	16.8	1.29
Pd-AC	1.94	1020	663	3.8	0	4.6	28.2	2.16

[a] Determined by ICP-OES. [b] Determined by *t*-plot method. [c] Calculated from desorption branch of N_2 sorption isotherm by BJH method. [d] Determined using elemental analysis. [e] Calculated based on TEM analysis. [f] Estimated on the basis of average Pd particle size calculated from TEM analysis and using equation described by Isaifan *et al.* (ref. 17). [g] Calculated assuming Pd metal particles as hemispherical in shape with the flat side on the support.

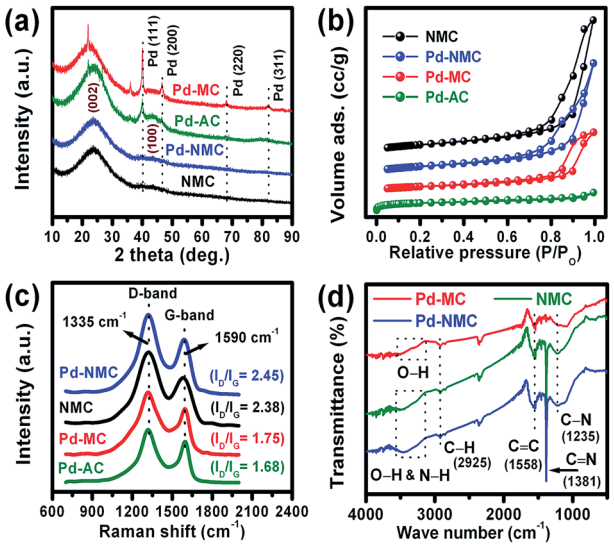

Fig. 1 (a) XRD pattern, (b) N_2 adsorption–desorption isotherm, (c) Raman spectra and (d) FT-IR spectra of NMC and Pd catalysts.

1590 cm^{-1}, respectively. The D-band reflects defects in carbons whereas the G-band indicates the graphitic structure of carbons.[15] The intensity ratios of the D-band to the G-band (I_D/I_G, calculated from integral area of the peaks) are 1.68, 1.75, 2.38 and 2.45 for Pd-AC, Pd-MC, NMC and Pd-NMC, respectively. The higher I_D/I_G ratios for nitrogen containing samples compared to nitrogen-free samples (Pd-AC and Pd-MC) shows that the incorporation of nitrogen in carbon frameworks led to more disordered structures.[15]

Fourier transform infrared (FT-IR) spectroscopy studies were carried out to identify the functional groups present in NMC, Pd-NMC and Pd-MC samples (Fig. 1d). The peak observed at 1558 cm^{-1} in all the samples was assigned to stretching vibration of C=C bonds of benzenoid ring.[14c,d] The peaks detected at 1381 and 1235 cm^{-1} in case of NMC and Pd-NMC corresponds to the stretching modes of C=N and C–N bonds, respectively.[14c,d] These peaks (1381 and 1235 cm^{-1}) were not seen in Pd-MC, which shows the absence of nitrogen in the Pd-MC. The peak at 2925 cm^{-1} is related to the stretching vibration of C–H bonds.[14d] The broad peak in the range of the 3150–3560 cm^{-1} detected in NMC and Pd-NMC were attributed to the stretching vibration of O–H and N–H bonds.[14c,d] Whereas, the peak (3150–3560 cm^{-1}) observed in Pd-MC were assigned to the O–H bonds stretching frequency.

In X-ray photoelectron spectroscopy (XPS) study of NMC, carbon, oxygen and nitrogen were detected while only carbon and oxygen were seen in MC (Fig. 2a). The N 1s spectra of NMC (Fig. 2b) are curve-fitted into three peaks with the binding energy values at 398.2, 400.4 and 401.8 eV that correspond to pyridinic N (N1), pyrrolic N (N2) and graphitic N (N3), respectively.[15] The Pd 3d XPS spectra of Pd-MC (Fig. 2c) and Pd-NMC (Fig. 2d) catalysts consist of two peaks related to Pd $3d_{5/2}$ and Pd $3d_{3/2}$. The peaks around 336.1 and 341.2 eV were assigned to metallic Pd (Pd^o), corresponding to Pd^o $3d_{5/2}$ and Pd^o $3d_{3/2}$, respectively.[10,13] Whereas, the peaks at 337.8 and 342.7 eV are attributed to the Pd in +2 oxidation state (PdO) and hence assigned to Pd^{2+} $3d_{5/2}$ and Pd^{2+} $3d_{3/2}$, respectively.[10,13] According to XPS data, the Pd^o percentage in Pd-NMC and Pd-MC were 86 and 65%, respectively. These results clearly suggest that the incorporation of nitrogen in the carbon framework resulted in the increased proportions of metallic Pd.[10,13]

The mesoporous structure of NMC and MC can be further confirmed by transmission electron microscopy (TEM) (Fig. 3), which revealed that both samples consists of randomly distributed spherical mesopores with disordered amorphous carbon structure. It can be seen that the Pd nanoparticles with an average size of 2.4 nm were homogeneously distributed throughout the NMC support (Fig. 4a and b). On the other hand, Pd nanoparticles were found to be dispersed unevenly and large agglomerated Pd nanoparticles were detected on the surface of MC and AC (Fig. 4c–f). The average particle sizes of Pd nanoparticles in Pd-MC and Pd-AC were found to be 7.7 and 4.6 nm, respectively. Hence, it can be concluded that the nitrogen dopant significantly contributes for the stabilization of Pd nanoparticles, thus leading to smaller Pd particles.[16]

The average particle size of Pd nanoparticles (calculated based on TEM analysis) on Pd-NMC, Pd-AC and Pd-MC catalysts were used to calculate dispersion (%) of Pd assuming spherical shape of particles and using the formula described by Isaifan *et al.*[17]

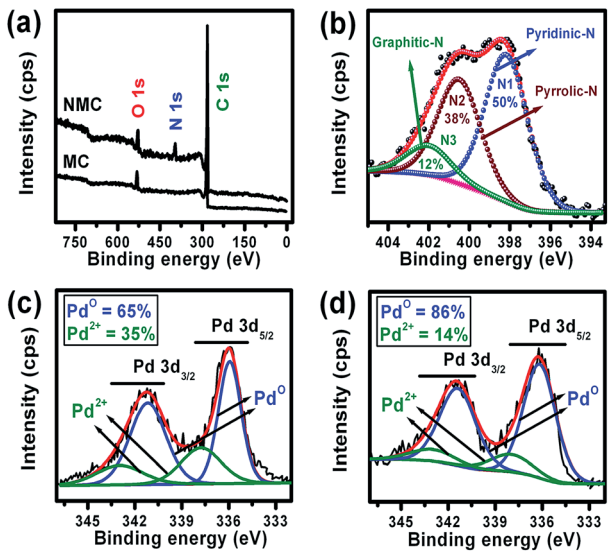

Fig. 2 (a) XPS survey of MC and NMC. (b) High resolution XPS spectra of N 1s for NMC. (c) XPS spectra of Pd 3d for Pd-MC. (d) XPS spectra of Pd 3d for Pd-NMC.

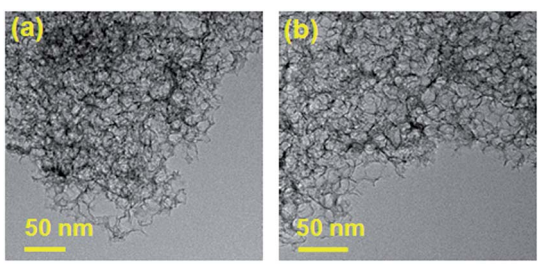

Fig. 3 TEM image of the (a) MC and (b) NMC.

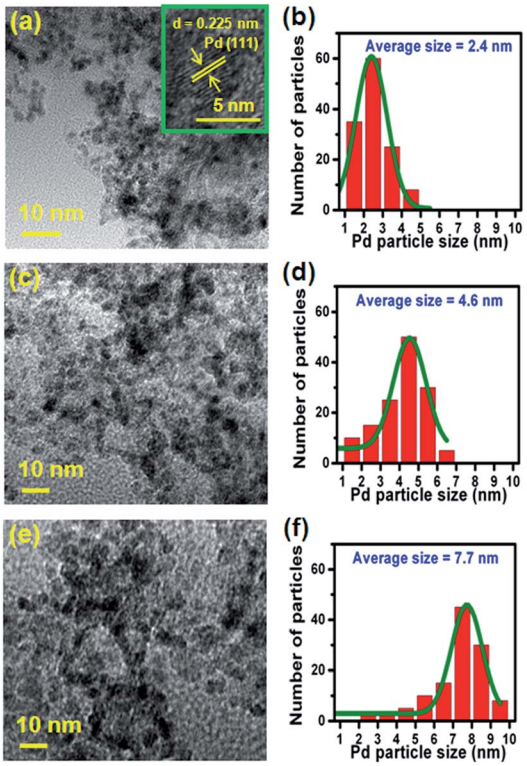

Fig. 4 TEM images and the Pd nanoparticles size distribution for Pd-NMC (a and b), Pd-AC (c and d) and Pd-MC (e and f), respectively.

(see ESI†). The Pd dispersion values were: Pd-NMC, 54%; Pd-MC, 16.8% and Pd-AC, 28.2% (Table 1). The higher dispersion of Pd in Pd-NMC confirms that nitrogen doping led to the homogeneous distribution of Pd nanoparticles over NMC support.

2.2. Catalytic activity in hydrogenation of CA to HCA

2.2.1. Effect of solvent. Solvent plays an important role in heterogeneous catalytic hydrogenations and possibly may alter the distribution of the products.[18] Hydrogenation of CA was carried out in polar–aprotic (acetonitrile), protic (ethanol and 2-propanol), non-polar (cyclohexane and toluene) and in water solvents. Table 2 provides the CA conversion and products selectivity data over Pd-NMC catalyst at 30 °C. The chemical and physical properties (polarity and H_2 solubility) of the solvents used are also given in Table 2. Under the reaction conditions studied, mainly HCA and 3-phenyl propanol (PPL) products were observed. The CA conversion was found to be relatively high in ethanol and 2-propanol compared to other solvents. On the other hand, lower CA conversion was seen in cyclohexane and toluene, possibly due to the poor solubility of reactants, including H_2 in these solvents (entry 2 and 3, Table 2). It is interesting to note that HCA selectivity was in the range of 81.2 to 93% in all the solvents. When 2-propanol was employed as solvent; comparatively high catalytic activity was witnessed. The 100% CA conversion was achieved within 3 h along with 93% HCA selectivity at a TOF value of 987 h^{-1} (entry 5, Table 2). Although, 2-propanol is known as a hydrogen transfer reagent, the results suggested that the effect of transfer hydrogenation was nil under the reaction conditions used (entry 6, Table 2). In case of water as solvent, low reactivity (TOF = 229 h^{-1}) with 23.2% CA conversion and 81.2% HCA selectivity was noticed (entry 7, Table 2). The inferior catalytic activity in water may be due to the poor solubility of H_2 in water (Table 2).[19] In this particular case, probably H_2 solubility along with solvent polarity are the vital factors. In view of the higher apparent activity and superior HCA selectivity (93%), 2-propanol was chosen as the solvent for further investigations.

2.2.2. Comparison of various supported Pd catalysts. To study the effect of the catalyst support, the Pd-NMC catalyst was compared with other catalysts including Pd-MC and Pd-AC under identical reaction conditions (30 °C and 5 bar H_2 pressure) and the results are given in the Fig. 5. Among the different catalysts studied, Pd-NMC exhibited relatively better hydrogenation activity affording 93% HCA selectivity with 100% CA conversion within 3 h. The HCA selectivity for MC and NMC-based Pd catalysts were almost stable, at 66 and 93%, respectively. However, HCA selectivity for AC-based Pd catalyst was decreased from 53 to 44% with increasing CA conversion. MC supported Pd nanoparticles were not effective for this reaction, resulting in low selectivity of desired product (HCA) with low CA conversion. The reason for this may be poor Pd dispersion and the larger size of Pd nanoparticles (7.7 nm). Similarly, Pd-AC catalyst showed low HCA selectivity, in spite of

Table 2 Hydrogenation of CA in different solvents over Pd-NMC[a]

					Products selectivity (%)			
Entry	Solvent	Solvent polarity index	H_2 solubility[b] (mmol L^{-1})	CA conv. (%)	HCA	PPL	Others[c]	TOF[d] (h^{-1})
1	Acetonitrile	5.8	—	71.2	88.3	11.7	0	702
2	Cyclohexane	0.2	3.72	43.5	91.1	8.9	0	429
3	Toluene	2.4	2.75	57.3	87.5	12.5	0	565
4	Ethanol	5.2	3.43	89.7	83.0	12.2	4.8	885
5	2-Propanol	3.9	3.90	100	93.0	4.9	2.1	987
6[e]	2-Propanol	3.9	3.90	—	—	—	—	—
7	Water	9.0	0.81	23.2	81.2	18.8	0	229

[a] Reaction conditions: CA (7.5 mmol); catalyst (Pd-NMC, 25 mg); solvent (25 mL); H_2 pressure (5 bar); time (3 h); temperature (30 °C); stirring speed (800 rpm). [b] H_2 solubility values in various solvents is taken from ref. 19. [c] Other products include acetal and ethers. [d] TOF = turnover frequency (moles of CA converted per mole of surface Pd per unit hour). [e] In the absence of H_2.

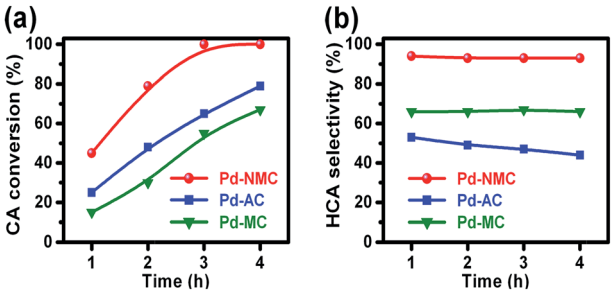

Fig. 5 (a) CA conversion and (b) HCA selectivity as a function of reaction time over different Pd catalysts. Reaction conditions: CA (7.5 mmol); catalyst (25 mg); solvent (2-propanol, 25 mL); H_2 pressure (5 bar); temperature (30 °C); stirring speed (800 rpm).

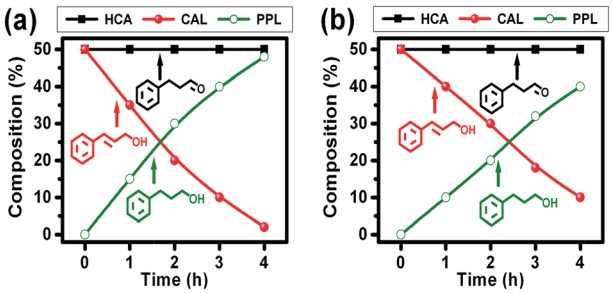

Fig. 6 Hydrogenation of HCA and CAL over (a) Pd-NMC and (b) Pd-AC catalyst as a function of reaction time. Reaction conditions: HCA (4 mmol); CAL (4 mmol); catalyst (25 mg); solvent (2-propanol, 25 mL); H_2 pressure (5 bar); temperature (30 °C); stirring speed (800 rpm).

having high surface area (1020 m^2 g^{-1}, Table 1) and PPL was obtained in considerable quantity. The high microporosity of AC (>60% of total surface area, Table 1) might be responsible for the poor diffusion of the reactant molecules and the hydrogenated products.[4a] Hence, hydrogenation reaction might have proceeded slowly with low HCA selectivity. The presence of acidic sites on AC could also modify the hydrogenation pathway leading to the loss in selectivity.[4a] The superior catalytic performance and improved C=C hydrogenation selectivity observed on N-doped Pd catalyst could be attributed to the following factors: (i) better Pd dispersion (54%) leading to higher Pd metal surface area (4.15 m^2 g^{-1}, Table 1) due to the presence of nitrogen, (ii) appropriate metal–support interaction between Pd and NMC support because of small Pd particle size, (iii) electronic activation of Pd nanoparticles by the nitrogen present in the support,[4d,13] as more Pd^0 seen from the XPS studies that might modify the adsorption mode of the CA and selectivity of the products,[20,21] and (iv) mesoporosity of NMC support that facilities free diffusion of the reactants and hydrogenated products.

Investigations were also conducted with Pd-NMC and Pd-AC catalysts using equimolar quantities of HCA and CAL as reactants, which are C=C and C=O hydrogenated product of CA, respectively (Fig. 6). The HCA was not further hydrogenated to PPL on both the catalysts under the reaction conditions used (30 °C and 5 bar H_2 pressure), which indicates that the re-adsorption of HCA molecule through the C=O bond did not occur on the Pd nanoparticles irrespective of the nature of the catalyst support. However, CAL was converted to PPL to a great extent on both the catalysts. The results shown in Fig. 5 and 6 clearly suggest that on Pd-AC, the CA must have adsorbed in such a way that almost simultaneous hydrogenation of the C=C and C=O bonds takes place whereas on the Pd-NMC catalyst the C=C hydrogenated product (HCA) were quickly desorbed from the active sites. These important observations point to the fact that all PPL obtained in CA hydrogenation under the reaction conditions studied actually formed *via* the formation of CAL as an intermediate. Notably, CAL was not detected in the reaction mixture, suggesting that CAL formed during the course of reaction must have rapidly converted to PPL. Similar observations were reported by Mahmoud *et al.*[2b] in CA hydrogenation over Pd/SiO_2 catalyst. They found that PPL was not formed from HCA in significant concentration at close to ambient temperature. Whereas, the hydrogenation of CAL to PPL proceeded nearly 30 times faster than the hydrogenation of CA to CAL.

The catalytic activity of NMC supported Pd (2 wt%) is significantly higher than that of Pd (5 wt%) supported on carbon nanofibers. With less amount of Pd in the NMC supported catalyst, 100% CA conversion was achieved only in 3 h at 30 °C, while it required nearly 30 h at 80 °C over the carbon nanofibers supported catalyst.[4a] Activated carbon supported Pd (10 wt%) catalyst converted 100% CA with 87% HCA selectivity under 40 bar H_2 pressure.[4c] Few-layer graphene supported Pd (5 wt%) catalyst showed nearly 100% CA conversion and 92% HCA selectivity at 80 °C.[4e] Nitrogen-doped carbon nanotubes supported Pd (10 wt%) catalyst offered almost 100% CA conversion with 90% HCA selectivity at 80 °C in 8 h.[4d] Therefore, it can be noticed that the Pd catalyst of the present study (Pd-NMC) is more efficient and the NMC support plays an important role in enhancing the catalytic activity.

2.2.3. Effect of reaction temperature. Influence of reaction temperature on the CA conversion and selectivity to various products was studied by changing the temperature in the 30–60 °C range over Pd-NMC catalyst at 5 bar H_2 pressure (Fig. 7). CA conversion was 100% with an excellent HCA selectivity (93%) within 3 h at ambient temperature (30 °C). At 40 and 50 °C, the CA hydrogenation rate was accelerated without any loss in HCA selectivity. For example, 100% CA conversion was achieved in 2.5 and 2 h at 40 and 50 °C, respectively. It is important to note that the HCA selectivity remains nearly constant (93%) even after 100% CA conversion was attained when the CA hydrogenation was carried out at lower temperatures (30, 40 and 50 °C). This leads to the conclusion that under the above reaction conditions the hydrogenation of HCA to PPL does not take place significantly. Otherwise, one would expect HCA selectivity to diminish with time. Notably, when the reaction temperature was further increased to 60 °C, a drop in HCA selectivity (from 88–72%) was witnessed. This reduction in HCA selectivity was attributed to the enhanced hydrogenation rate of HCA to PPL at higher temperature. These observations are in good agreement with the literature, which reports that the over Pd catalyst hydrogenation of HCA does not yield any detectable amount of PPL at lower temperatures.[2b] And the hydrogenation of HCA to PPL was increased at higher reaction temperature.

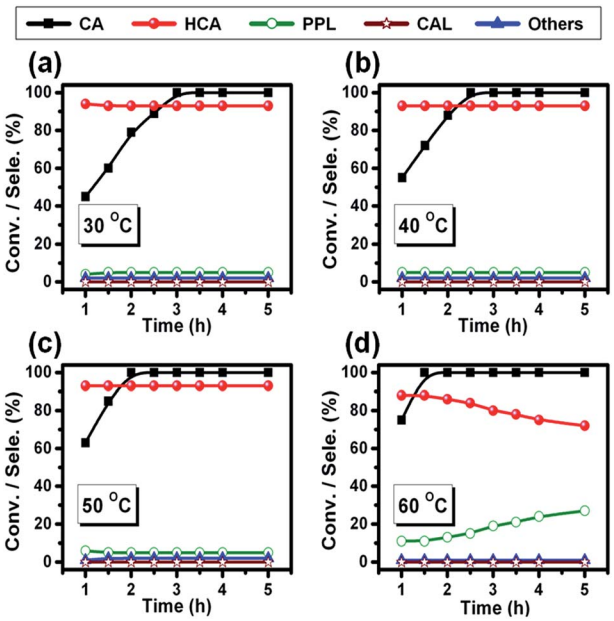

Fig. 7 Effect of reaction temperature (a) 30 °C, (b) 40 °C, (c) 50 °C and (d) 60 °C, on CA conversion and products selectivity as a function of reaction time. Reaction conditions: CA (7.5 mmol); catalyst (Pd-NMC, 25 mg); solvent (2-propanol, 25 mL); H_2 pressure (5 bar); stirring speed (800 rpm).

2.2.4. Effect of H_2 pressure. Influence of H_2 pressure on the CA hydrogenation was studied by varying the pressure in the range of 1–5 bar over Pd-NMC catalyst at 30 °C (Fig. 8). The CA conversion was improved from 40 to 100%, when the H_2 pressure was increased from 1 to 5 bar. But, the HCA selectivity was not significantly altered and remained nearly at 93%. Hence, 5 bar H_2 pressure was considered as optimum to get 100% CA conversion and 93% HCA selectivity in 3 h. However, even at 1 bar H_2 pressure, similar conversion and selectivity can be achieved on prolonging the reaction time (9 h).

2.2.5. Possible reaction mechanism. There is a relationship between metal d-band width and the product selectivity's in the hydrogenation of α,β-unsaturated carbonyl compounds.[2a,22] The Huckel calculations suggest that the narrower the metal d-band width, larger the interaction of the metal surface with the conjugated C=C bond compared to the C=O bond.[23] The width of the metal d-band increases in the following order: Pd < Pt < Ir ≈ Os.[23] Therefore, the chemisorption of C=C bond becomes more favorable over the Pd metal catalysts. DFT calculations have revealed that the maleic anhydride interacts with the Pd (111) surface through the C=C bond.[24] Over the Pd-NMC catalyst, the C=C bond in CA molecule may get adsorbed almost parallel to the Pd metal surface as a results of small particle size of Pd nanoparticles (2.4 nm). Most probably, the close interaction between C=C bond and the Pd metal surface may lead to superior catalytic performance. Scheme 2 demonstrates the proposed step sequence in the chemoselective hydrogenation of CA. In the first step, CA interacts with the Pd surface through the C=C bond and H_2 molecule is dissociated over electronically promoted Pd (due to presence of nitrogen as observed through XPS studies). Subsequently, the selective hydrogenation of C=C bond occurs by the attack of the activated hydrogen species. As a result of the presence of mesoporous channels in the NMC support, the formed saturated carbonyl (HCA) rapidly leaves the catalyst surface and is replaced with a new reactant (CA) molecule. This avoids further hydrogenation of HCA to saturated alcohol (PPL).

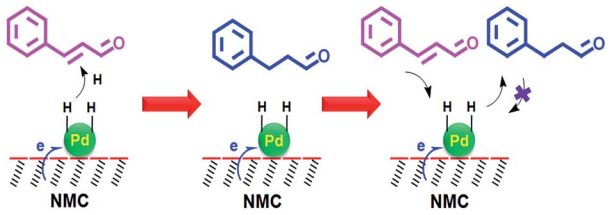

Scheme 2 Possible reaction mechanism for the selective hydrogenation of CA to HCA over Pd-NMC catalyst.

2.2.6. Recyclability study. The recyclability of the Pd-NMC catalyst in the CA hydrogenation was investigated by repeating the reaction with the same catalyst without any regeneration or activation (Fig. 9). Pd-NMC was found to be active even after six recycles without any significant drop in activity and HCA

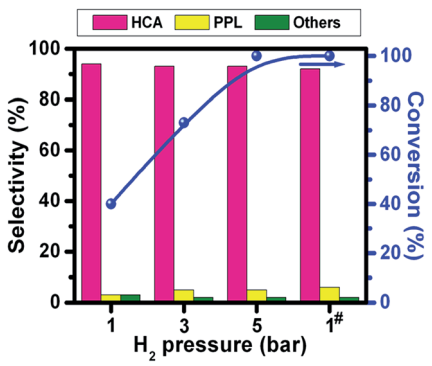

Fig. 8 Effect of H_2 pressure on CA hydrogenation. Reaction conditions: CA (7.5 mmol); catalyst (Pd-NMC, 25 mg); solvent (2-propanol, 25 mL); temperature (30 °C); time (3 h, # 9 h); stirring speed (800 rpm).

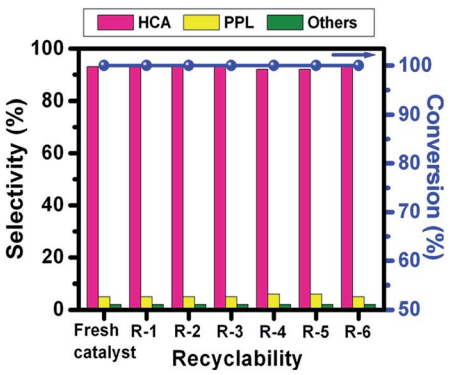

Fig. 9 Recyclability study of Pd-NMC catalyst in the CA hydrogenation. Reaction conditions: molar ratio of CA to Pd (1600); solvent (2-propanol, 25 mL); H_2 pressure (5 bar); time (3 h); temperature (30 °C); stirring speed (800 rpm).

selectivity, which is a prerequisite for practical industrial applications. In order to gain more insight into the catalytic activity during recycle study, XRD and TEM analysis of spent catalysts were carried out. XRD results showed that the catalyst did not undergo any change during the reaction (Fig. S1, ESI†). The TEM image of the Pd-NMC after six recycles exhibited an average Pd nanoparticles size of 2.6 nm, almost the same as that of the fresh catalyst (Fig. S2, ESI†). These results demonstrate an excellent stability of the catalyst. The reaction mixture after each recycle was analyzed using ICP-OES for the presence of Pd, due to leaching. No Pd was observed, indicating strong interaction between the Pd and NMC support. In addition, the amount of Pd in the catalyst after six recycles was similar to that of the starting catalyst.

3. Conclusions

Chemoselective liquid-phase hydrogenation of CA was investigated over Pd supported on NMC, MC and AC catalysts. Catalyst Pd-NMC showed admirable catalytic activity and high HCA selectivity (93%) under mild reaction conditions (30 °C, 5 bar H_2). It could be reused for over six cycles without any loss in activity and selectivity. This good catalytic performance is attributed to the presence of nitrogen in the carbon framework and mesoporous nature of the support. The mesoporous structure of NMC support helps better mass transfer of the reactant molecules to the active sites and promotes the free diffusion of the hydrogenated products. The incorporation of nitrogen atoms in the carbon network not only leads to a very stable and homogeneous dispersion of Pd nanoparticles but also responsible for electronic and morphologic modifications of the active phase. The synthesis approach used in this study (incorporation of heteroatoms in the catalyst support) may help to design various other catalysts, which may be useful for the production of numerous fine chemicals.

4. Experimental section

4.1. Chemicals

All chemicals used were reagent grade and employed without further purification. Acetonitrile, cyclohexane, toluene, ethanol, 2-propanol, melamine, phenol, formaldehyde, NaOH, $NaBH_4$, $AgNO_3$, CA (98%), HCA (98%), CAL (98%) and PPL (98%) were procured from Loba Chemie, Mumbai. Whereas, Ludox SM-30 colloidal silica (30 wt% SiO_2 in water), $PdCl_2 \cdot 2H_2O$ and AC were purchased from Alfa Aesar.

4.2. Synthesis of catalysts

4.2.1. Synthesis of NMC. The NMC support was synthesized *via* a colloidal silica assisted sol–gel process by using melamine as a nitrogen source (Scheme S1, ESI†).[15] In a typical synthetic procedure, 3.67 g of phenol (39 mmol) and 6.33 g of formaldehyde (37 wt%, 78 mmol) were added drop-wise to 50 mL of NaOH solution (0.2 M, 10 mmol) under stirring. The mixture was stirred at room temperature for 20 min and then heated in an oil bath at 70 °C under stirring for 40 min. To it, 9.84 g of melamine (78 mmol) and another part of formaldehyde (12 g) were added with continuous stirring for 30 min. Then, 50 g of Ludox SM-30 sol (30 wt% SiO_2) was added to the above solution to react for 1 h with consecutive agitation. The suspension was then transferred to sealed bottle and heated at 80 °C for 3 days. The obtained gel was dried at 80 °C and the material obtained was grinded in mortar. This powder was carbonized in N_2 flow at 800 °C for 3 h while heating at the rate of 5 °C min^{-1}. The final NMC was obtained by dissolution of the silica in 2 M NaOH solution at 80 °C for 12 h. The resulting material was washed with distilled water until pH is neutral and dried at 100 °C for 10 h. The nitrogen-free mesoporous carbon (MC) was also prepared by using above process without adding any melamine content.

4.2.2. Synthesis of Pd-NMC. The 2 wt% Pd-NMC catalyst was synthesized by a modified ultrasonic-assisted method (Scheme S2, ESI†).[13] Typically, 0.1 g of NMC was dispersed in 50 mL of deionized water in 100 mL round bottom flask by ultrasonication (20 min). To it, 0.5 mL of aqueous $PdCl_2$ solution (Pd content 4 mg mL^{-1}) was added under ultrasonication. This mixture was stirred at 80 °C for 6 h and cooled to room temperature. Then, aqueous $NaBH_4$ ($Pd/NaBH_4 = 1:4$ mol mol^{-1}) was added to the above solution drop-wise under ultrasonication for 30 min. The solution was filtered and washed with deionized water until no chloride ions were detected (confirmed by $AgNO_3$ test). The resulting 2 wt% Pd-NMC catalyst was dried in an oven at 80 °C for 10 h and used for catalytic tests. Catalysts 2 wt% Pd-MC and 2 wt% Pd-AC were also prepared by following above procedure.

4.3. Characterization techniques

The physico-chemical characterizations of the samples were carried out by using various techniques such as powder XRD, N_2 sorption, FT-IR, Raman, ICP-OES, TEM and XPS. Further details are provided in the ESI.†

4.4. Evaluation of catalysts

All the reactions were carried out using a 100 mL Parr autoclave (SS316). In a typical experiment, CA (7.5 mmol), 25 mL of solvent and the desired amount of freshly reduced catalyst was introduced into the reactor vessel. The reactor contents were mixed thoroughly and the reactor was sealed, purged two to three times with hydrogen and pressurized to required hydrogen pressure. Afterward, the reaction was carried out at required temperature with continuous stirring (800 rpm). Liquid samples were withdrawn periodically and analyzed using GC (Agilent 7890A) equipped with a flame ionization detector having CP Sil 8 CB capillary column (30 m length, 0.25 mm diameter). Product identification was done using authentic standards and by using GC-MS (Shimadzu, GCMS-QP2010 Ultra; HP-5 column; 30 m length, 0.25 mm diameter).

Acknowledgements

Atul S. Nagpure and Lakshmiprasad Gurrala acknowledge Council of Scientific and Industrial Research (CSIR), New Delhi, for

providing senior research fellowships. Authors also acknowledge financial support from CSIR Network project CSC-0122.

References

1 (*a*) M. Boudart, *Nature*, 1994, **372**, 320; (*b*) P. Gallezot and D. Richard, *Catal. Rev.: Sci. Eng.*, 1998, **40**, 81; (*c*) P. Claus, *Top. Catal.*, 1998, **5**, 51; (*d*) U. K. Singh and M. A. Vannice, *Appl. Catal., A*, 2001, **213**, 1.

2 (*a*) P. Maki-Arvela, J. Hajek, T. Salmi and D. Y. Murzin, *Appl. Catal., A*, 2005, **292**, 1; (*b*) S. Mahmoud, A. Hammoudeh, S. Gharaibeh and J. Melsheimer, *J. Mol. Catal. A: Chem.*, 2002, **178**, 161.

3 (*a*) A. J. Plomp, H. Vuori, A. O. I. Krause, K. P. de Jong and J. H. Bitter, *Appl. Catal., A*, 2008, **351**, 9; (*b*) Z.-T. Liu, C.-X. Wang, Z.-W. Liu and J. Lu, *Appl. Catal., A*, 2008, **344**, 114; (*c*) A. Jung, A. Jess, T. Schubert and W. Schuetz, *Appl. Catal., A*, 2009, **362**, 95; (*d*) A. Solhy, B. F. Machado, J. Beausoleil, Y. Kihn, F. Goncalves, M. F. R. Pereira, J. J. M. Orfao, J. L. Fiqueiredo, J. L. Faria and P. Serp, *Carbon*, 2008, **46**, 1194; (*e*) S. Takenaka, T. Iguchi, E. Tanabe, H. Matsune and M. Kishida, *Catal. Lett.*, 2011, **141**, 821; (*f*) J. Lenz, B. C. Campo, M. Alvarez and M. A. Volpe, *J. Catal.*, 2009, **267**, 50; (*g*) M. L. Toebes, F. F. Prinsloo, J. H. Bitter, A. J. van Dillen and K. P. de Jong, *J. Catal.*, 2003, **214**, 78; (*h*) J. Hajek, N. Kumar, P. Maki-Arvela, T. Salmi, D. Yu. Murzin, I. Paseka, T. Heikkila, E. Laine, P. Laukkanen and J. Vayrynen, *Appl. Catal., A*, 2003, **251**, 385; (*i*) B. F. Machado, H. T. Gomes, P. Serp, P. Kalck and J. L. Faria, *ChemCatChem*, 2010, **2**, 190; (*j*) J. P. Breen, R. Burch, J. Gomez-Lopez, K. Griffin and M. Hayes, *Appl. Catal., A*, 2004, **268**, 267; (*k*) C. Wang, J. S. Qiu, C. H. Liang, L. Xing and X. M. Yang, *Catal. Commun.*, 2008, **9**, 1749; (*l*) V. S. Gutierrez, A. S. Diez, M. Dennehy and M. A. Volpe, *Microporous Mesoporous Mater.*, 2011, **141**, 207; (*m*) Z. Liu, Y. Yang, J. Mi, X. Tan and Y. Song, *Catal. Commun.*, 2012, **21**, 58.

4 (*a*) C. Pham-Huu, N. Keller, G. Ehret, L. J. Charbonniere, R. Ziessel and M. J. Ledoux, *J. Mol. Catal. A: Chem.*, 2001, **170**, 155; (*b*) B. H. Zhao, J. G. Chen, X. Liu, Z. W. Liu, Z. Hao, J. Xiao and Z. T. Liu, *Ind. Eng. Chem. Res.*, 2012, **51**, 11112; (*c*) F. Zhao, Y. Ikushima, M. Chatterjee, M. Shirai and M. Arai, *Green Chem.*, 2003, **5**, 76; (*d*) J. Amadou, K. Chizari, M. Houlle, I. Janowska, O. Ersen, D. Begin and C. Pham-Huu, *Catal. Today*, 2008, **138**, 62; (*e*) T. Truong-Huu, K. Chizari, I. Janowska, M. S. Moldovan, O. Ersen, L. D. Nguyen, M. J. Ledoux, C. Pham-Huu and D. Begin, *Catal. Today*, 2012, **189**, 77; (*f*) A. M. R. Galletti, C. Antonetti, A. M. Venezia and G. Giambastiani, *Appl. Catal., A*, 2010, **386**, 124; (*g*) H. Wang, Y. Shu, M. Zheng and T. Zhang, *Catal. Lett.*, 2008, **124**, 219; (*h*) A. J. Marchi, D. A. Gordo, A. F. Trasarti and C. R. Apesteguía, *Appl. Catal., A*, 2003, **249**, 53.

5 T. Vergunst, F. Kapteijn and J. A. Moulijn, *Catal. Today*, 2001, **66**, 381.

6 (*a*) M. Antonietti and K. Mullen, *Adv. Mater.*, 2010, **22**, 787; (*b*) Y. Wan, H. Wang, Q. Zhao, M. Klingstedt, O. Terasaki and D. Zhao, *J. Am. Chem. Soc.*, 2009, **131**, 4541; (*c*) Y. Hao, G.-P. Hao, D.-C. Guo, C.-Z. Guo, W.-C. Li, M.-R. Li and A.-H. Lu, *ChemCatChem*, 2012, **4**, 1595.

7 (*a*) R. J. White, R. Luque, V. L. Budarin, J. H. Clark and D. J. Macquarrie, *Chem. Soc. Rev.*, 2009, **38**, 481; (*b*) F. Clippel, M. Dusselier, R. Van Rompaey, P. Vanelderen, J. Dijkmans, E. Makshina, L. Giebeler, S. Oswald, G. V. Baron, J. F. M. Denayer, P. P. Pescarmona, P. A. Jacobs and B. F. Sels, *J. Am. Chem. Soc.*, 2012, **134**, 10089.

8 S. Crossley, J. Faria, M. Shen and D. E. Resasco, *Science*, 2010, **327**, 68.

9 V. Z. Radkevich, T. L. Senko, K. Wilson, L. M. Grishenko, A. N. Zaderko and V. Y. Diyuk, *Appl. Catal., A*, 2008, **335**, 241.

10 Y. Wang, J. Yao, H. Li, D. Su and M. Antonietti, *J. Am. Chem. Soc.*, 2011, **133**, 2362.

11 L. Zhao, L.-Z. Fan, M.-Q. Zhou, H. Guan, S. Qiao, M. Antonietti and M.-M. Titirici, *Adv. Mater.*, 2010, **22**, 5202.

12 K. P. Gong, F. Du, Z. H. Xia, M. Durstock and L. M. Dai, *Science*, 2009, **323**, 760.

13 X. Xu, Y. Li, Y. Gong, P. Zhang, H. Li and Y. Wang, *J. Am. Chem. Soc.*, 2012, **134**, 16987.

14 (*a*) W. Yang, T. P. Fellinger and M. Antonietti, *J. Am. Chem. Soc.*, 2011, **133**, 206; (*b*) P. F. Fulvio, J. S. Lee, R. T. Mayes, X. Q. Wang, S. M. Mahurin and S. Dai, *Phys. Chem. Chem. Phys.*, 2011, **13**, 13486; (*c*) Z. Ma, H. Zhang, Z. Yang, G. Ji, B. Yu, X. Liu and Z. Liu, *Green Chem.*, 2016, **18**, 1976; (*d*) G.-P. Hao, W.-C. Li, D. Qian and A.-H. Lu, *Adv. Mater.*, 2010, **22**, 853.

15 H. Chen, F. Sun, J. Wang, W. Li, W. Qiao, L. Ling and D. Long, *J. Phys. Chem. C*, 2013, **117**, 8318.

16 X. Xie, J. Long, J. Xu, L. Chen, Y. Wang, Z. Zhang and X. Wang, *RSC Adv.*, 2012, **2**, 12438.

17 R. J. Isaifan, H. A. E. Dole, E. Obeid, L. Lizarrag, P. Vernoux and E. A. Baranova, *Electrochem. Solid-State Lett.*, 2012, **15**(3), E14–E17.

18 (*a*) R. J. Hou, T. F. Wang and X. C. Lan, *Ind. Eng. Chem. Res.*, 2013, **52**, 13305; (*b*) S. Mukherjee and M. A. Vannice, *J. Catal.*, 2006, **243**, 108.

19 (*a*) Z. Wei, Y. Gong, T. Xiong, P. Zhang, H. Li and Y. Wang, *Catal. Sci. Technol.*, 2015, **5**, 397; (*b*) M.-M. Wang, L. He, Y.-M. Liu, Y. Cao, H.-Y. He and K.-N. Fan, *Green Chem.*, 2011, **13**, 602; (*c*) S. Fujiwara, N. Takanashi, R. Nishiyabu and Y. Kubo, *Green Chem.*, 2014, **16**, 3230.

20 R. Schlogl, Surface composition and structure of active carbon, in *Handbook of Porous Solids*, ed. F. Schuth, K. S. W. Sing and J. Weitkamp, Wiley–VCH, 2002, pp. 1863–1900.

21 C. Pham-Huu, N. Keller, G. Ehret and M. J. Ledoux, *J. Catal.*, 2001, **200**, 400.

22 Y. A. Ryndin, C. C. Santini, D. Prat and J. M. Basset, *J. Catal.*, 2000, **190**, 364.

23 F. Delbecq and P. Sautet, *J. Catal.*, 1995, **152**, 217.

24 V. Pallassana, M. Neurock and G. W. Coulston, *J. Phys. Chem. B*, 1999, **103**, 8973.

